Adaptive Vibration Attenuation with Globally Convergent Parameter Estimation

Mohammad Abdollahpouri*, Gabriel Batista, Gergely Takács, Tor Arne Johansen, and Boris Rohaľ-Ilkiv

M. Abdollahpouri, G. Batista, G. Takács and B. Rohaľ-Ilkiv are with the Slovak University of Technology in Bratislava, Faculty of Mechanical Engineering, Institute of Automation, Measurement and Applied Informatics, Nám. Slobody 17, 812 31 Bratislava 1, Slovakia.

T. A. Johansen is with the Center for Autonomous Marine Operations and Systems (NTNU-AMOS), Department of Engineering Cybernetics, Norwegian University of Science and Technology, 7491 Trondheim, Norway.

Abstract

Parameter estimation problems can be nonlinear, even if the dynamics are expressed by a linear model. The extended Kalman filter (EKF), even though it is one of the most popular nonlinear estimation techniques, may not converge without sufficient a priori information. This paper utilizes a globally convergent nonlinear estimation method—the double Kalman filter (DKF)—for a vibrating cantilever beam. A globally valid linear time-varying (LTV) model is required by the first stage of the DKF depending on some conditions on input and output excitation. Without considering noise, this LTV model provides the first stage and is globally equivalent to the nonlinear system. Since the neglected input and output noises can degrade the quality of estimation, the second stage linearizes the nonlinear dynamics, utilizing the nominally globally convergent estimate of the first stage, and improves the quality of estimation. Both estimation methods were applied to a cantilever beam setup in real-time. An adaptive linear quadratic regulator utilizes the estimated parameters to attenuate unknown transient disturbances. Different scenarios have been explored, providing a fair comparison between EKF and DKF. These methods have been implemented on an embedded ARM-based microcontroller unit and illustrates improved convergent properties of the DKF over the EKF. The global stability of the DKF is verified and it has been observed that it needs twice the computational cost of the EKF.

Keywords: joint state and parameter estimation problem, globally convergent Kalman filtering, real-time embedded implementation, adaptive vibration attenuation.

1. Introduction

The extended Kalman filter (EKF) has been proven to be an efficient nonlinear state estimation technique in many applications. It has been without a doubt the most popular state estimation technique in different

*Mohammad Abdollahpouri is currently affiliated with the Chalmers University of Technology in Göteborg, Sweden. (e-mail: mohammad.abdollahpouri@chalmers.se)

engineering applications; for instance in the field of robotics and mechanical systems, see [1], [2] and [3]. Its simple and practical algorithm depends on linearized state space models, and by proper tuning, its performance is sometimes comparable to sophisticated estimation techniques such as the moving horizon estimation [4], even though inherently EKF can not deal with constraints in its design. Basically, EKF is the solution to a least-squared optimization problem [5] and since it is incorporating nonlinear dynamics, in general, it is reasonable to expect existence of several local minimums or sub-optimal solutions.

Although EKF performs reliably in a nominal scenario, its fundamental drawback originates from the internal feedback loop; i.e. utilizing the estimated state as a linearization point. This feature, even though it simplifies the method in practical sense, makes EKF sensitive to erroneous initial guesses and/or wrong tuning parameters. This means that EKF can begin with a wrong initial guess, which is used to construct a trajectory for calculating the linearized model and consequently ends up with instability. Divergence of the EKF has been reported; see [6, 7, 8, 9, 10]. In other words, it is clear that EKF is not globally convergent, but it might not even be locally convergent; see [11, 12] for an example. In this paper, a globally convergent estimation method achieves the conventionally true estimates for an arbitrary choice of initial state. On the other hand, a locally convergent estimation technique would require a region of states in which the initial state must be selected to guarantee convergence. Even though the initial state and tuning parameters for a nominal operating point can be selected properly, a sudden change in the structure of system dynamics might create a wrong linearization point for EKF, which potentially results in divergence. Here, we will investigate some of these scenarios in detail and propose a globally convergent estimation technique to adaptively attenuate the vibration of a cantilever beam.

Cascaded Kalman filters making use of two ore more algorithm stages have been proposed before ; e.g. in [13, 14] the authors developed a dual Kalman filter for linear time-varying systems to prevent the numerical issues regarding unobservability and rank deficiency of the estimation problem. In the topic of nonlinear state and parameter estimation, a novel type of two stage state estimation approach has been recently introduced in [15], where the first stage (auxiliary estimator) provides a linearization point for the second stage. One of its variants, the double Kalman filter (DKF), has been analyzed in the continuous-time domain [16] and its global stability properties in discrete-time have been studied in [17]. Furthermore, its performance has been evaluated by a simulation study using pseudo-range measurements for position estimation [12].

The first stage of DKF employs a technique, which eliminates nonlinearities of the system using a model transformation that results in a linear time-varying (LTV) model. This model reformulation uses previous outputs and control inputs without optimally considering the input and output disturbances. Suboptimal modeling of disturbances degrades the performance, hence the second stage, a linearized Kalman filter (LKF), utilizes estimates from the first stage as its linearization point. Compared to EKF, where the previously calculated estimates define a linearization trajectory, DKF makes use of a globally convergent estimation technique in its first stage as auxiliary Kalman filter (AKF), which uses the transformed LTV

model to provide the second stage with useful information for linearization; independent from the result of LKF. While technically an entire class of cascaded estimation algorithms consisting of two Kalman filter stages can be called *double*, in this paper we will use the term double Kalman filter to refer only to the combination of a first stage based on a LTV model (the AKF) that is augmented by a linearized Kalman filter (the LKF) as its second stage.

This configuration actually prevents the instability mechanisms of internal feedback, which can otherwise result in divergence for an estimation method such as EKF. Other popular nonlinear estimation methods, such as the moving horizon estimation (MHE) [4] and the unscented Kalman filtering (UKF) [18, 19, 20] are locally convergent in their nominal design. Since MHE in general is solving a non-convex optimization problem, the existence of several local solutions is expected. Also the divergence properties of the UKF has been studied in [6].

From the implementation point of view, limited resources means limited model complexity and simplified algorithms. A vibrating cantilever beam is the case study we consider in this paper and its parameters are going to be estimated and supplied to a linear quadratic regulator (LQR) for adaptive vibration attenuation. This structure may, for example, represent a flexible wing; see [21]. In these vibrating structures the scale of change in dynamics is significantly longer than the chosen sampling period.

Basically, any system can be described by a complicated nonlinear model, however, sometimes even a simple model can result in computational complexity, that is intractable for applied control problems. As we will later show, the application of such a model in control and estimation is on the verge of not being real-time feasible on current embedded microcontrollers, hence a linear model has been adopted to demonstrate the behavior of the beam, creating a joint state and parameter estimation problem that is nonlinear.

In this paper we derive a globally nominally equivalent LTV model that fully represents the original nonlinear parameter estimation problem for a vibrating structure represented by a single degree-of-freedom model. The existence of this LTV model relies on the persistent excitation (PE) of input and output signals, which is detailed in Sect. 2.

Furthermore, to the best knowledge of the authors, this paper presents the first experimental real-time validation of the DKF method. In addition to the real-time feasibility study itself, this work takes a look at an embedded application of the DKF on a microcontroller unit (MCU); foreshadowing its possibilities and limitations in low-cost applications.

We put forward an adaptive vibration control scheme in Sect. 3 making use of the proposed LTV model in a DKF parameter estimation algorithm that is combined with control. Convergence issues and practical performance of both EKF and DKF have been investigated through different implementation scenarios, and are described in Sect. 4.

The experimental validation of this cascade estimation configuration with a LQR controller is demonstrated on a 32-bit ARM Cortex-M4 architecture MCU. The timing analysis provides an insight in the

computational complexity regarding different estimation and control techniques.

Structural changes and external additive measurement noise have also been emulated to contrast the behavior of the two estimation techniques in the adaptive vibration control of the structure in Sect. 5.

2. Model transformation

A vibrating cantilever beam can be described by nonlinear partial differential equations in general. However, for small deflections we may use the linear model, since the dynamics of a highly flexible cantilever is dominated by its first resonant frequency. Such flexible structures are often described by simple second order linear models [22, 23]. It should be noted that a linear model including higher non-dominant frequencies can be used but is not feasible to be implemented on a typical MCU. With only one extra higher frequency involved (one extra measurement will be needed), the number of augmented states will double in size. Therefore, this extra burden for computational complexity is not feasible for our assigned MCU and we utilize the following simple model for estimation and control:

$$\dot{x}_1(t) = x_2(t), \tag{1a}$$

$$\dot{x}_2(t) = -\omega_n^2(t)x_1(t) - 2\xi(t)\omega_n(t)x_2(t) + \alpha(t)u(t). \tag{1b}$$

The displacement of the beam is denoted by x_1 and the corresponding velocity is expressed by x_2. The control input, or in the case of free vibration, the excitation signal, is denoted by u. The parameters, natural frequency ω_n [rad/s], proportional damping ξ [-] and input gain α [N/V], along with the states and input signal are assumed to be time-varying (functions of time t). Compared to a LTI model with time invariant parameters, this assumption helps the simple LTV model (1) to be valid for a wider range of operating systems. In the context of joint state and parameter estimation it is common to augment the state vector with parameters evolving slowly with time according to a Wiener process. This assumption makes it possible to augment the states with parameters as the following nominal nonlinear model

$$\dot{x}_1(t) = x_2(t), \tag{2a}$$

$$\dot{x}_2(t) = x_1(t)x_3(t) + x_2(t)x_4(t) + x_5(t)u(t), \tag{2b}$$

$$\dot{x}_3(t) = 0, \tag{2c}$$

$$\dot{x}_4(t) = 0, \tag{2d}$$

$$\dot{x}_5(t) = 0, \tag{2e}$$

$$y(t) = x_1(t), \tag{2f}$$

where $x_3(t) = -\omega_n^2(t)$, $x_4(t) = -2\xi(t)\omega_n(t)$ and $x_5(t) = \alpha(t)$ are augmented states corresponding to respective parameters. In equation (2) the only known values are the measurement that is denoted by $y(t)$ and

the control input $u(t)$, hence all the augmented parameters (x_3, x_4 and x_5) and the tip-mass velocity ($x_2(t)$) are unknown. It should be noted that process noise will be added to the nominal model (2) in order to describe the time-varying and stochastic nature of the expected parameter variations. The properties of the additive process noise, needs to be adjusted properly. In an adaptive control framework or an estimation algorithm, this augmentation makes it possible to calculate the updated parameters at the same time with time-varying states.

Implementing any model-based control or estimation algorithm on an embedded MCU requires the dynamic model in discrete time. In order to simplify the notation, we make use of x_k^i to represent the i^{th} state at time instance k[2]; hence using Euler integration with sampling time T_s, the following discrete time model is valid

$$x_{k+1}^1 = x_k^1 + T_s x_k^2, \tag{3a}$$
$$x_{k+1}^2 = T_s x_k^1 x_k^3 + (1 + T_s x_k^4) x_k^2 + T_s x_k^5 u_k, \tag{3b}$$
$$x_{k+1}^3 = x_k^3, \tag{3c}$$
$$x_{k+1}^4 = x_k^4, \tag{3d}$$
$$x_{k+1}^5 = x_k^5, \tag{3e}$$
$$y_k = x_k^1. \tag{3f}$$

It should be noted that even a different explicit integration scheme can be used with the model transformation. However, an implicit integration scheme might lead to additional computational complexity. Furthermore, the main challenge in using this augmented model in the estimation tasks is, having the multiplicative nonlinearity between states (displacement and velocity) and parameters (augmented states). In order to translate the state equation (3) to a LTV model, we utilized the approach presented in [17].

To this end, it is necessary to obtain all elements of x_k based on measurements. Re-writing (3a) one sample backward ($k \to k-1$) gives $x_k^1 = x_{k-1}^1 + T_s x_{k-1}^2$. Furthermore, using (3f) one can calculate $x_{k-1}^2 = (y_k - y_{k-1})/T_s := dy_k$. The same procedure can be used for (3b) as follows

$$\begin{aligned} x_k^2 &= T_s x_{k-1}^1 x_{k-1}^3 + (1 + T_s x_{k-1}^4) x_{k-1}^2 + T_s x_{k-1}^5 u_{k-1}, \\ &= T_s y_{k-1} x_k^3 + (1 + T_s x_k^4) dy_k + T_s x_k^5 u_{k-1}, \end{aligned} \tag{4}$$

where the parameters are assumed to be constant over a small number of sampling periods. It is necessary to do these steps three more times. Therefore, we can write $x_{k-j}^1 = y_{k-j}$ and $x_{k-j-1}^2 = dy_{k-j}$ for $j = 0, 1, \ldots, 4$.

[2]The upper numerical indices in this paper are not powers, instead denote the state formulation element index.

Re-writing (4) one sample backward in a sequential way, gives

$$\begin{aligned} x^2_{k-1} =& T_s x^1_{k-2} x^3_{k-2} + (1 + T_s x^4_{k-2}) x^2_{k-2} + T_s x^5_{k-2} u_{k-2}, \\ \rightarrow dy_k =& T_s y_{k-2} x^3_k + (1 + T_s x^4_k) dy_{k-1} + T_s x^5_k u_{k-2}, \qquad (5) \\ \rightarrow dy_{k-1} =& T_s y_{k-3} x^3_k + (1 + T_s x^4_k) dy_{k-2} + T_s x^5_k u_{k-3}, \qquad (6) \\ \rightarrow dy_{k-2} =& T_s y_{k-4} x^3_k + (1 + T_s x^4_k) dy_{k-3} + T_s x^5_k u_{k-4}. \qquad (7) \end{aligned}$$

Let us assume that u_{k-2}, u_{k-3} and u_{k-4} are also known, so we can solve the linear system for x^3_k, x^4_k and x^5_k described by (5)–(7) as follows

$$\begin{bmatrix} x^3_k \\ x^4_k \\ x^5_k \end{bmatrix} = \frac{1}{T_s} \begin{bmatrix} y_{k-2} & dy_{k-1} & u_{k-2} \\ y_{k-3} & dy_{k-2} & u_{k-3} \\ y_{k-4} & dy_{k-3} & u_{k-4} \end{bmatrix}^{-1} \begin{bmatrix} dy_k - dy_{k-1} \\ dy_{k-1} - dy_{k-2} \\ dy_{k-2} - dy_{k-3} \end{bmatrix}, \qquad (8)$$

where the existence of matrix inversion will be analyzed in two cases below. If it exists, unknown parameters based on the previous measurements and controls will be obtained as

$$\begin{bmatrix} x^3_k \\ x^4_k \\ x^5_k \end{bmatrix} := \begin{bmatrix} \phi_3(\mathcal{Y}^k_{k-4}, \mathcal{U}^{k-2}_{k-4}) \\ \phi_4(\mathcal{Y}^k_{k-4}, \mathcal{U}^{k-2}_{k-4}) \\ \phi_5(\mathcal{Y}^k_{k-4}, \mathcal{U}^{k-2}_{k-4}) \end{bmatrix}, \qquad (9)$$

where

$$\begin{aligned} \phi_3(\mathcal{Y}^k_{k-4}, \mathcal{U}^{k-2}_{k-4}) =& \frac{1}{\Delta_k} \Big((y_{k-1} - y_{k-3}) \big(u_{k-2}(y_{k-3} - y_{k-4}) + \\ & u_{k-4}(y_{k-2} - y_{k-1}) \big) - (y_{k-2} - y_{k-4}) \big(u_{k-2}(y_{k-2} - y_{k-3}) + \\ & u_{k-3}(y_{k-2} - y_{k-1}) \big) - (y_k - y_{k-2}) \big(u_{k-3}(y_{k-3} - y_{k-4}) + \\ & u_{k-4}(y_{k-3} - y_{k-2}) \big) \Big), \\ \phi_4(\mathcal{Y}^k_{k-4}, \mathcal{U}^{k-2}_{k-4}) =& \frac{1}{\Delta_k} \Big((y_k - y_{k-2})(u_{k-3} y_{k-4} - u_{k-4} y_{k-3}) \\ & -((y_{k-1} - y_{k-3})(u_{k-2} y_{k-4} - u_{k-4} y_{k-2})) + \\ & ((y_{k-2} - y_{k-4})(u_{k-2} y_{k-3} - u_{k-3} y_{k-2})) \Big), \\ \phi_5(\mathcal{Y}^k_{k-4}, \mathcal{U}^{k-2}_{k-4}) =& \frac{1}{\Delta_k} \Big((y_{k-1} y_{k-4} - y_{k-2} y_{k-3}) \\ & (y_{k-1} - y_{k-3}) - ((y_{k-2} - y_{k-4})(-y^2_{k-2} + y_{k-1} y_{k-3})) - \\ & (y_k - y_{k-2})(-y^2_{k-3} + y_{k-2} y_{k-4}) \Big). \end{aligned}$$

The determinant is $\Delta_k = u_{k-2}(y^2_{k-3} - y_{k-4} y_{k-2}) + u_{k-3}(y_{k-1} y_{k-4} - y_{k-2} y_{k-3}) + u_{k-4}(y^2_{k-2} - y_{k-1} y_{k-3})$, $\mathcal{Y}^j_i$ is a set of measurements from y_i to y_j, and $\mathcal{U}^j_i$ is a set of controls from u_i to u_j for $j \geq i$.

Case 1: The value of Δ_k can be zero, when no input and no output excitation exists. In this scenario ϕ_3, ϕ_4 and ϕ_5 are ill-posed. Therefore, a condition on the existence of a non-zero Δ_k is crucial. This is similar to the PE condition on signals, where the the matrix of data is defined in (8); see [24].

Case 2: With no input signal, but with non-zero output signal; e.g. near the steady-state mode of a possible adaptive control scenario, u_k will be calculated as zero, hence Δ_k becomes zero. In this scenario, the estimator could freeze the fifth parameter associated with ϕ_5 to the previously calculated value, and the reduced problem assumes a fixed α, hence (8) converts to

$$\begin{bmatrix} x_k^3 \\ x_k^4 \end{bmatrix} = \frac{1}{T_s} \underbrace{\begin{bmatrix} y_{k-2} & dy_{k-1} \\ y_{k-3} & dy_{k-2} \end{bmatrix}}_{A_y}^{-1} \begin{bmatrix} dy_k - dy_{k-1} \\ dy_{k-1} - dy_{k-2} \end{bmatrix} \tag{10}$$

where its existence does not depend on the input anymore. It should be noted that in this scenario the input gain parameter can not estimated anymore. Also, in practice during the steady-state mode, control is not applied, so this estimated parameter causes no harm to the adaptive control strategy.

Remark 2.1. *To be able to use* (10)*, it is necessary to investigate the rank of* A_y*. In practice* (3f) *becomes* $x_k^1 = y_k - v_k$ *and* $x_{k-1}^2 = dy_k + dv_k$*, where* $dv_k = (v_k - v_{k-1})/T_s$*. Re-writing* (5) *and* (6) *gives*

$$\begin{aligned} dy_k + dv_k =& T_s(y_{k-2} + v_{k-2})x_k^3 + (1 + T_s x_k^4)(dy_{k-1} + dv_{k-1}) + T_s x_k^5 u_{k-2}, \\ dy_{k-1} + v_{k-1} =& T_s(y_{k-3} + v_{k-3})x_k^3 + (1 + T_s x_k^4)(dy_{k-2} + dv_{k-2}) + T_s x_k^5 u_{k-3}, \end{aligned}$$

and therefore, (10) *becomes*

$$\begin{bmatrix} x_k^3 \\ x_k^4 \end{bmatrix} = \frac{1}{T_s} \begin{bmatrix} y_{k-2} + v_{k-2} & dy_{k-1} + dv_{k-1} \\ y_{k-3} + v_{k-3} & dy_{k-2} + dv_{k-2} \end{bmatrix}^{-1} \begin{bmatrix} dy_k - dy_{k-1} + dv_k - dv_{k-1} \\ dy_{k-1} - dy_{k-2} + dv_{k-1} - dv_{k-2} \end{bmatrix}. \tag{11}$$

Therefore for the steady-state case, even if y_{k-2} *and* y_{k-3} *are zero, by assuming a Gaussian white measurement noise,* (11) *is almost always well-posed, as the rank condition is*

$$rank(A_y) = rank(\begin{bmatrix} v_{k-2} & v_{k-1} \\ v_{k-3} & v_{k-2} \end{bmatrix}) = 2,$$

which means A_y *is full rank, since in general* v_j *and* v_{j-1} *are assumed to be uncorrelated. However, it should be noted that this does not mean that some kind of observability is defined, since noise has no information for estimation tasks, hence it does not imply that parameter estimates will converge with zero excitation. Hence, the experiments are designed in a way to avoid the aforementioned cases. It will be shown by experiments in Sect. 5 that the existence of* A_y*, which depends on the output excitation was not an issue, and it was always well-posed during our tests.* □

Remark 2.2. *From a practical point of view, estimation/adaptation must be disabled in steady-state mode, since there is no point of control in such cases. Also, PE condition in real-life applications (e.g. plane wing) is usually satisfied and the system can typically do not go to a perfect steady-state; there will usually be some mechanical excitations.* □

Using (9) we can obtain x_k^2 from (4) as a function of previous measurements and controls

$$\begin{aligned} x_k^2 =& T_s y_{k-1}\phi_3(\mathcal{Y}_{k-4}^k, \mathcal{U}_{k-4}^{k-2}) + (1 + T_s\phi_4(\mathcal{Y}_{k-4}^k, \mathcal{U}_{k-4}^{k-2}))dy_k \\ &+ T_s\phi_5(\mathcal{Y}_{k-4}^k, \mathcal{U}_{k-4}^{k-2})u_{k-1} := \phi_2(\mathcal{Y}_{k-4}^k, \mathcal{U}_{k-4}^{k-1}, T_s) \end{aligned}$$

and this makes it possible to transform the model (3), without any approximation in dynamics to a LTV model as follows

$$x_{k+1} = F(\mathcal{Y}_{k-4}^k, \mathcal{U}_{k-4}^k)x_k + G(\mathcal{Y}_{k-4}^k, \mathcal{U}_{k-4}^k)u_k, \tag{12}$$

where the matrices F and G in (12) are given as

$$F = \begin{bmatrix} 1 & T_s & 0 & 0 & 0 \\ (1-\eta)T_s\phi_3 & 1 + (1-\eta)T_s\phi_4 & \eta T_s y_k & \eta T_s\phi_2 & \eta T_s u_k \\ 0 & 0 & 1 & 0 & 0 \\ 0 & 0 & 0 & 1 & 0 \\ 0 & 0 & 0 & 0 & 1 \end{bmatrix}$$

$$G = \begin{bmatrix} 0 & (1-\eta)T_s\phi_5 & 0 & 0 & 0 \end{bmatrix}^{\mathrm{T}},$$

where $\eta \in \mathbb{R}$ is a free parameter and for simplicity its value is selected as 0.5; it should be noted that this value does not influence the validity of the transformed model, and merely demonstrate that it is not unique. Furthermore, the arguments of functions $\phi_j(\cdot,\cdot)$ for $j = 2,3,4,5$ are not given in (12) for brevity. It should be noted that $F(\cdot,\cdot)$ and $G(\cdot,\cdot)$ in (12) are known time-varying matrices. Also, in our case study, the measurement function is linear ($y_k = Cx_k$, where $C = \begin{bmatrix} 1 & 0 & 0 & 0 & 0 \end{bmatrix}$). For the rest of the paper, the LTV system matrices will be denoted by F_k and G_k.

The method presented here is indeed scalable and how it is carried out varies case by case, since at the moment a formal treatment of this approach is not developed yet. In [17] some stability properties have been studied, which can be useful for moving this research forward. In this paper, our goal was to demonstrate the real-time feasibility of this method for microcontroller deployment. Considering two physical state (tip-mass displacement and its velocity) and three time-varying parameters, the augmented system has 5 states. Since one sensor is employed (for measuring the tip-mass displacement), it has been demonstrated that 5 steps of previous and current measurements is required; $\{\mathcal{Y}_{k-4}^k,\ \mathcal{U}_{k-4}^k\}$. One can argue that if a more sophisticated model is employed (for example including more dominant vibration modes) the number of

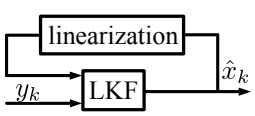

(a) Scheme of the EKF

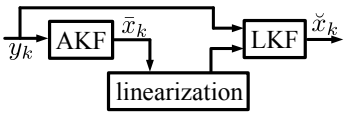

(b) Scheme of the DKF

Figure 1: Estimation schemes

steps in the window of measurement will increase. However, similar to the discussion provided in Remark 2.1, equation (8) needs to be checked for the rank deficiency and the existence of the matrix inversion.

3. Adaptive vibration attenuation scheme

This section summarizes the estimation techniques that have been utilized in the adaptive control framework. Algorithms with low complexity are given, that need minimum effort for being deployed to an embedded system. Furthermore, the adaptive LQR formulation is described. It is necessary to point out that the control method is not in focus here, rather its performance depending on the convergence of estimated parameters is our main interest.

3.1. EKF

The extended Kalman filter—an extension to the classical Kalman Filter (KF)—deals with nonlinear dynamics by linearizing it about the previously calculated estimates; see Fig. 1a. Let us denote the nonlinear dynamics of the vibration system given by (3) as follows

$$x_{k+1} = f(x_k, u_k) + w_k, \tag{13a}$$

$$y_k = Cx_k + v_k, \tag{13b}$$

where $f(\cdot,\cdot)$ is the nonlinear state dynamics, and the input and output disturbances are denoted by w_k and v_k, respectively. To implement the EKF, Alg. 1 can be employed [25]. Within this estimation approach, $\hat{x}_k$ is the estimated state. This algorithm starts with obtaining the required initial guess for state vector as x_0 and its covariance matrix P_0. Similar to the KF, it is assumed that the input and output disturbances are Gaussian (see [25]), hence the covariance of input and output disturbances are selected as Q_0 and R_0, respectively. The Kalman gain $\hat{K}$ is updated at each sample time and the current estimated state $\hat{x}_k$ will be given by measuring the current input u_k and output y_k.

3.2. DKF

A double Kalman filter is basically the cascade configuration of two linear KFs. The first stage—auxiliary KF—(AKF) utilizes the transformed globally valid LTV model in (12), and the second stage (LKF) linearizes the nonlinear dynamics (3) about the result of AKF; see Fig. 1b. The most important drawback of AKF

Algorithm 1 Implementation of EKF

Initialization: $\hat{x} = x_0$, $\hat{P} = P_0$, $Q = Q_0$ and $R = R_0$

Input: y_k and u_k

1: Update $A = \frac{\partial f(x,u)}{\partial x}\big|_{x=\hat{x},u=u_k}$

2: $\hat{P} \leftarrow A\hat{P}A^{\mathrm{T}} + Q$

3: $\hat{x} \leftarrow f(\hat{x}, u_k)$

4: $\hat{K} \leftarrow \hat{P}C^{\mathrm{T}}(C\hat{P}C^{\mathrm{T}} + R)^{-1}$

5: $\hat{P} \leftarrow (I - \hat{K}C)\hat{P}(I - \hat{K}C)^{\mathrm{T}} + \hat{K}R\hat{K}^{\mathrm{T}}$

6: $\hat{x} \leftarrow \hat{x} + \hat{K}(y_k - C\hat{x})$

Output: $\hat{x}_k = \hat{x}$

is, that during the model transformation described in Sect. 2, w_k and v_k in (13), are not considered in the equations. Hence, the following system expresses the model that the AKF utilizes

$$x_{k+1} = F_k x_k + G_k u_k + \acute{w}_k, \tag{14a}$$

$$y_k = Cx_k + v_k, \tag{14b}$$

where $\acute{w}_k$ has different properties than w_k. In a nutshell, (13) and (14) give

$$\acute{w}_k = w_k + f(x_k, u_k) - (F_k x_k + G_k u_k),$$

and considering the fact that F_k and G_k depend on measurements, and these values are noisy as well (see (13b)), deriving the properties of $\acute{w}_k$ is a formidable task. It should be also noted, that even if w_k is assumed to be Gaussian and white, $\acute{w}_k$ will have a different density function and not be white anymore. The AKF still uses the assumption that $\acute{w}_k$ stays Gaussian and white but with a different covariance matrix $\bar{Q}_0$, while the covariance matrix of w_k is supposed to be Q_0 as it was for EKF. Since there was no transformation needed for the output function, the properties of v_k stay the same for AKF and EKF.

The second stage of the DKF is necessary to compensate for the effect of the transformation of the input disturbance ($\acute{w}_k$). To this end, we linearize the nonlinear system in (13) about the state estimate $\bar{x}_{k|k}$ of the first stage of the DKF, which gives

$$x_{k+1} = f(\bar{x}_{k|k}, u_k) + A_k(x_k - \bar{x}_{k|k}) + \mathcal{Q}_k + w_k, \tag{15a}$$

$$y_k = C_k x_k + v_k, \tag{15b}$$

where $A_k = \frac{\partial f}{\partial x}(\bar{x}_{k|k}, 0)$, while $\mathcal{Q}_k = [\mathcal{Q}_{1,k}, \ldots, \mathcal{Q}_{n,k}]^{\mathrm{T}}$ is the higher order remainder term due to linearization and from [26]

$$\mathcal{Q}_{i,k} = (x_k - \bar{x}_{k|k})^{\mathrm{T}} \left(\int_0^1 (1-s) \frac{\partial^2 f_i}{\partial x \partial x^{\mathrm{T}}}(sx_k + (1-s)\bar{x}_{k|k}, u_k) \mathrm{d}s \right) (x_k - \bar{x}_{k|k}), \tag{16}$$

for all $i \in \{1, \ldots, n\}$, where f_i is the i^{th} element of f. We note that w_k is uniformly zero if $\acute{w}_k$ is uniformly zero. Furthermore, from [17, 16], there exist constants $\epsilon_q, \epsilon_r \in \mathbb{R}_{>0}$ such that

$$\|\mathcal{Q}_k\| \leq \epsilon_q \|x_k - \bar{x}_{k|k}\|^2, \quad \|\mathcal{R}_k\| \leq \epsilon_r \|x_k - \bar{x}_{k|k}\|^2,$$

for $k \geq 0$. This means that the higher order terms will vanish asymptotically, if the estimates of the first stage are uniformly globally asymptotically stable ($x_k - \bar{x}_{k|k} \to 0$).

The LKF formulation about $\bar{x}_{k|k}$ as an operating point is

$$\breve{K}_k = \breve{P}_{k|k-1} C_k^{\mathrm{T}} (C_k \breve{P}_{k|k-1} C_k^{\mathrm{T}} + R_k)^{-1}, \tag{17a}$$

$$\breve{x}_{k|k} = \breve{x}_{k|k-1} + \breve{K}_k (y_k - C_k \breve{x}_{k|k-1}), \tag{17b}$$

$$\breve{P}_{k|k} = (I - \breve{K}_k C_k) \breve{P}_{k|k-1}, \tag{17c}$$

with initial conditions $\breve{x}_{0|-1}$ and $\breve{P}_{0|-1}$. These initial conditions and the measurement noise covariance matrix R_k are typically the same as in the EKF and AKF, and $\breve{K}_k$ is the Kalman gain. The propagation for the state estimate is as follows

$$\breve{x}_{k+1|k} = f(\bar{x}_{k|k}, u_k) + A_k (\breve{x}_{k|k} - \bar{x}_{k|k}), \tag{18a}$$

$$\breve{P}_{k+1|k} = A_k \breve{P}_{k|k} {A_k}^{\mathrm{T}} + Q_k, \tag{18b}$$

where the process noise covariance matrix Q_k is utilized in EKF formulation. To perform this estimation in real-time see Alg. 2, while considering cases 1 and 2 in Sect. 2.

3.3. Adaptive LQR

The linear quadratic regulator (LQR) is one of the most popular full state feedback controllers; e.g. see [27] and [28]. This paper focuses on the estimation tasks and control is only considered as a validation tool, thus it should be noted that estimation results can be easily utilized in any other full state feedback controller. After the estimates have been obtained, the system dynamics is no longer nonlinear and (3) can be simplified to a LTV model as follows

$$x_{k+1} = \begin{bmatrix} 1 & T_s \\ T_s \tilde{x}_k^3 & (1 + T_s \tilde{x}_k^4) \end{bmatrix} x_k + \begin{bmatrix} 0 \\ T_s \tilde{x}_k^5 \end{bmatrix} u_k := \tilde{A}_k x_k + \tilde{B}_k u_k, \tag{19a}$$

where $\tilde{x}$ in this scenario can be replaced by either of the estimates within EKF or DKF. It should be noted, that these parameters are time varying, hence LQR needs to be updated at each sampling time, and the implementation details of this adaptive controller are given in Alg. 3. In this algorithm, N_{LQ} is the finite time horizon that is selected for the LQR. The terms Q_{LQ} and R_{LQ} are the stage deviation and input usage weighting matrices in the cost term, respectively. In order to reduce the computational complexity we make use of a finite horizon formulation, which utilizes the solution of a discrete-time dynamic Riccati equation

Algorithm 2 Implementation of DKF

Initialization: $\breve{x} = \bar{x} = x_0$, $\bar{P} = \breve{P} = P_0$, $\bar{Q} = \bar{Q}_0$, $\breve{Q} = Q_0$ and $R = R_0$

Input: $y_k, \ldots, y_{k-L}$ and $u_k, \ldots, u_{k-L}$

Update F_k and G_k from (12).

$\bar{P} \leftarrow F_k \bar{P} F_k^{\mathrm{T}} + \bar{Q}$

$\bar{x} \leftarrow F_k \bar{x} + G_k u_k$

$\bar{K} \leftarrow \bar{P} C^{\mathrm{T}} (C \bar{P} C^{\mathrm{T}} + R)^{-1}$

$\bar{P} \leftarrow (I - \bar{K} C) \bar{P} (I - \bar{K} C)^{\mathrm{T}} + \bar{K} R \bar{K}^{\mathrm{T}}$

$\bar{x} \leftarrow \bar{x} + \bar{K}(y_k - C\bar{x})$ {END of AKF}

Update $A_k = \frac{\partial f(x,u)}{\partial x}\big|_{x=\bar{x}, u=0}$

$\breve{P} \leftarrow A_k \breve{P} A_k^{\mathrm{T}} + \breve{Q}$

$\breve{x} \leftarrow f(\bar{x}, u_k) + A_k(\breve{x} - \bar{x})$

$\breve{K} \leftarrow \breve{P} C^{\mathrm{T}} (C \breve{P} C^{\mathrm{T}} + R)^{-1}$

$\breve{P} \leftarrow (I - \breve{K} C) \breve{P} (I - \breve{K} C)^{\mathrm{T}} + \breve{K} R \breve{K}^{\mathrm{T}}$

$\breve{x} \leftarrow \breve{x} + \breve{K}(y_k - C\breve{x})$ {END of LKF}

Output: $\breve{x}_k = \breve{x}$

backward in time; see [29, 30, 31] for more details on discrete-time LQR. It's worth mentioning that, even though a infinite horizon LQR might seems to be less computationally demanding, a code generation tool was required for the real-time implementation. On the other hand, the finite horizon LQR was employed without any external tool and the resulting algorithm was less complex than infinite horizon LQR.

Algorithm 3 Implementation of LQR

Initialization: N_{LQ}, Q_{LQ} and R_{LQ}

Input: $\tilde{x}_k$

Update $\tilde{A}_k$ and $\tilde{B}_k$ in (19) and set $P_{N_{\mathrm{LQ}}} = Q_{\mathrm{LQ}}$

for $i = N_{\mathrm{LQ}}, \ldots, 1$ **do**

  $\tilde{P}_{i-1} = \tilde{A}^{\mathrm{T}} \tilde{P}_i \tilde{A} - \tilde{A}^{\mathrm{T}} \tilde{P}_i \tilde{B} (\tilde{B}^{\mathrm{T}} \tilde{P}_i \tilde{B})^{-1} \tilde{B}^{\mathrm{T}} \tilde{P}_i \tilde{A} + Q_{\mathrm{LQ}}$

end for

$F_0 = (R_{\mathrm{LQ}} + \tilde{B}_k^{\mathrm{T}} P_0 \tilde{B})^{-1} \tilde{B}_k^{\mathrm{T}} P_1 \tilde{A}_k$

Output: $u_k = -F_0 \tilde{x}_k$

4. Experimental implementation

4.1. Hardware implementation

Figure 3a presents the hardware scheme of the experiment. The aim of the adaptive control was to attenuate the transient vibration of an aluminum cantilever beam with removable tip-mass, shown on Fig. 2a. The dimensions of the beam were 550 mm×40 mm×3 mm. Two symmetrically placed MIDÉ QuickPack 16n piezoceramic transducers were used as actuators glued onto the fixed end of the cantilever beam. These actuators were powered by a MIDÉ EL 1225 power amplifier providing a gain of 20 V/V. A stinger mechanism made of a linear actuator was used to introduce a repeatable initial disturbance to the system. This type of disturbance is common to test aerospace structures, as it resembles transient vibration effects [32, 33, 34]. The position of the beam was measured by an optical measurement system consisting of a Keyence KL-G32 laser head and Keyence LK-3001V processing unit.

These systems were connected to a STM32F407 Discovery evaluation board, depicted on Fig. 2b, which was used as the main processing unit of the controller. The MCU used on the board was the STM32 F407VGT6 running at the nominal voltage of 3 V. This MCU uses an ARM-Cortex M4 core clocked at 168 MHz and has 128 kB of RAM and 1024 kB of ROM. The laser sensor has been setup so, that it converts the displacement to voltage signal in the range of 0–3 V with the conversion ratio of 10 mm/V. This was connected to the 12bit analog-to-digital (ADC) converter of the MCU. The input signal of the system was generated by the 12bit digital-to-analog converter (DAC) present on the MCU. This generated unipolar voltage also in the range of 0–3 V, which was then amplified and shifted to ±5 V and connected to the power amplifier. The stinger mechanism was connected to a general purpose input-output pin of the controller controlling the pulse of the stinger. Programming and data-logging was performed by a PC connected to the board using a serial link. The data-logging ran at a baud rate of 115200 which was sufficient to send 32 bytes of data in 3 ms. This way, the sampling period has been set to 15 ms which proved to be sufficient for this application.

4.2. Software implementation

The software for this application was written in plain C. The hardware driver code was generated using STM32F4 CubeMX V4.17.0 MCU code generation software provided by the manufacturer of the MCU. Here, the hardware specific F4 Firmware Package V1.13.2 has been utilized to setup the system clock, GPIO pins, ADC and DAC channels, serial communication and the necessary hardware timers. One hardware timer was setup to measure the execution timing of the control and estimation with the resolution of 10^{-5} s. The code was compiled using GCC for ARM V5.4.1 and then deployed to the memory of the chip using STLINK V1.1.0.

5. Results

This section provides the implementation results on the active cantilever beam setup. First, an open loop estimation task was performed to compare the effect of initial guess for the EKF and DKF. Next, the online estimation results were applied to the adaptive LQR to attenuate external disturbances. Furthermore, extra additive measurement noise has been emulated in order to investigate the behavior of DKF and EKF. Finally, a timing analysis provides an insight on how different tasks were accomplished within a sample period.

5.1. Comparison of estimation tasks

In this experiment, the consequences of wrong initial state on the estimation tasks are investigated. In order to do so, the configuration in Fig. 3b is employed. The PRBS signal was generated by an external signal generator, and it was read by the MCU as an analog input. The experiment starts with an additional weight on the tip mass and in the middle of the experiment it was detached from the tip mass. It should be noted that in all the following experiments, the time scale of parameter change is slower than the sampling time. The dominant free natural frequency of this vibrating beam is about 50 [rad/sec] and this value decreases to 20 with an extra tip-mass of 400 [g]. Therefore, an initial state guess of $x_0 = \{0.01, 0, -500, -1, 0.01\}$ is considered as close to the true values and the performance of EKF and DKF are almost indistinguishable; c.f. Fig. 4a. In Fig. 4b the choice of $x_0 = \{0.01, 0, -50000, -10, 0.01\}$ is shown to be a value that de-stabilizes the EKF, while the DKF demonstrates its convergent property. For the scenario, in which the initial guess is close to the true values, estimation covariance matrix is selected as $P_0 = \text{diag}\{0.1, 1, 200, 200, 0.1\}$, while for the other scenario it is considered as $P_0 = \text{diag}\{0.1, 1, 2 \times 10^5, 1000, 0.1\}$. This difference is due to the larger uncertainty in the choice of initial state and to help the estimators for a better convergence. The covariance matrix of process noise for AKF is $\bar{Q}_0 = \text{diag}\{0.1, 100, 1 \times 10^{10}, 100, 100\}$ in both cases, and this value for EKF and LKF is selected as $Q_0 = \text{diag}\{0.1, 100, 8 \times 10^9, 100, 10\}$ (note the difference between Q_0 and $\bar{Q}_0$ in order to compensate the approximation in model transformation). Note that $\text{diag}(\cdot)$ represents the diagonal matrix. The selection criteria for this matrix is based on the value of the state and parameters and their variance. Typically their variance provides an insight on the starting guess, while further trial and error is needed to obtain a tuning which provides the best estimation performance. Finally, the measurement noise variance is assumed to be $R_0 = 0.001$ in all cases and is selected based on the precision of the laser sensor for measuring the displacement. It is worth mentioning, that the estimated parameters are not assumed to be known and merely define the system behavior in (1). Since estimation results are obtained from the experimental data in an online fashion and no simulated model has been used for generating data for estimation tasks, the knowledge about the true value of the parameters does not have a meaning for the experimental study shown here. Based on Fig. 4b, it seems as if P_0 was chosen too small for the given wrong

Table 1: Estimation performance comparison with PRBS signal; see Fig. 4

Estimation methods	true initial guess			wrong initial guess		
	ω_n	ξ	α	ω_n	ξ	α
AKF	19.65	0.026	0.0001	19.8	0.024	-0.0004
DKF	20	0.026	0.0005	19.9	0.023	-0.0005
EKF	19.8	0.027	0.0004	N/A	N/A	N/A

x_0, however, even with a larger P_0 estimation diverges and EKF estimates were not a number (N/A) after 13 seconds. For the sake of clarity, it should be pointed out that for a better initialization (specifically by selecting $x_0(3) > -50000$), similar results were obtained as it was illustrated in Fig. 4a. Furthermore, the extremely incorrect initialization was designed to show, that there is a point where the nonlinear nature of EKF will result in divergence, while DKF can handle even such extreme issues due to its global convergence properties. Besides the initialization, there are other cases when sudden changes may drive EKF unstable, such as sensor malfunction.

To this end, a numerical comparison is provided in Table. 1, where the average of estimated parameters in steady-state during $2-15$ seconds are illustrated. Furthermore, note that the input gain parameter might become negative during some experiments depending on how the attached extra tip mass is inserted, and since the piezoelectric patches are positioned symmetrically its sign might be different. Similar as in all the following experiments, the tuning parameters were chosen to obtain the best estimation performance.

5.2. Adaptive LQR

In this experiment, estimation and control are performed at the same time, meaning that the control does not wait for estimation to converge, hence the transient response is influencing the control. In Fig. 3b the implementation sequence of estimation and control is illustrated. At each sampling period, displacement of the beam was measured and after estimating the parameters, a control action was calculated.

During the experiment, the beam has been excited twice using the stinger. This created an excitation that is enough for estimation methods to converge. After the vibration has been attenuated for the first time (after about 2 [s]), the tip mass was modified (augmented by 21 [g]) at approximately 10 seconds and another disturbance was injected. The estimation tuning parameters were fixed as $P_0 = \text{diag}\{0.1, 1, 200, 100, 10\}$, $\bar{Q}_0 = \text{diag}\{0.1, 100, 6 \times 10^9, 1000, 10\}$, $Q_0 = 1, 10, 4 \times 10^9, 1000, 10$ and $R_0 = 0.001$. The controller parameters as explained by Alg. 3 are $N_{\text{LQ}} = 50$, $Q_{\text{LQ}} = I_2$ and $R_{\text{LQ}} = 0.001$.

In Fig. 5a, the parameter estimation results are illustrated. Even though the initial guess is not very far from expected values, EKF can not converge to them (see the proportional damping coefficient ξ, where its value for EKF is negative), which mainly is because of not having sufficient excitation output; compare

it with the results in Sect. 5.1. Figure 5b demonstrates how the controller is providing enough excitation signal to attenuate the unknown disturbances provided by the stinger. Free oscillation is denoted by gray line and the performance of DKF is clearly better that the one of EKF.

5.3. Disturbance attenuation

It has been explained in Sect. 3.2 that AKF is not designed optimally considering measurement and process noises. Therefore, it is expected that the first stage of DKF performs weaker in the presence of additive measurement noise. In this scenario, two types of measurement noise with variance of $0.1[mm]$ have been emulated artificially via a signal generator; see Fig. 3b. In the design of EKF and LKF it is expected that process and measurement noises are Gaussian and white, while in AKF this assumption does not hold even theoretically. Therefore, as expected, the performance of AKF is quite different than the one of EKF and LKF; see Fig. 6. Since the only purpose of AKF is providing LKF with a linearization point, its performance loss is not so effective on LKF and we could not arrange a scenario in which DKF diverges beyond a relatively small bias; in order to make DKF divergent we need an additive noise with large amplitude, which makes the experiment impractical. On the other hand, an extra measurement noise with uniform distribution has a similar effect on all the estimation methods; see Fig. 7. In this situation, bias in all the methods (including EKF) for parameter ω_n is small but visible. As for the input gain parameter (α), AKF performs worse than other methods. It should be noted, that other amplitudes of additive measurement noise has been considered as well, but the results were not clear and we couldn't find a scenario, where DKF fails beyond relatively small biases. In all the experiments in this test, the estimation error covariance matrix was selected as $P_0 = \text{diag}\{0.1, 1, 2 \times 10^4, 100, 10\}$. The process noise covariance matrix for AKF was chosen as $\bar{Q}_0 = \text{diag}\{0.1, 100, 5 \times 10^9, 100, 1000\}$, while the same parameter for EKF and LKF was $Q_0 = \text{diag}\{1, 10, 6 \times 10^9, 1000, 10\}$. Considering the extra measurement noise, the covariance matrix for this term was selected as $R = 0.1$.

5.4. Computational load analysis

Timing analysis on an MCU is crucial, to keep the real-time constraint satisfied, even though the algorithms are quite simple. The computational complexity and also the storage need of DKF was almost twice of what we can see from EKF and this is considered as the main drawback of the DKF. This has been shown by estimation execution time (EET) in Table 2. These values demonstrate the time that has been spent on performing the estimation algorithms. Also the total execution time (TET) considers the time that was needed to execute the estimation task, control and data logging. By reducing TET from EET, we can calculate the time that is needed for executing the LQR plus the fixed 2.3 [ms] needed for data logging through the serial port. It is worth mentioning that he main equation that is utilized by the DKF (in both stages) is the discretized model (13). Therefore, the DKF is valid for any discrete time model, no matter

what type of explicit integration scheme is used. Regarding the computational time, it should be noted that even with a simple forward Euler integration method, the implementation of the adaptive vibration attenuation on the chosen MCU is on the verge of being real time feasible, so considering e.g. an implicit integration scheme would be most probably not real-time feasible.

Note that the execution time for EKF is significantly lower than a two staged KF. By comparing Alg. 1 and 2, EKF has less matrix evaluations to perform, hence its lower computational complexity is justified. Please see Alg. 2 to see why a DKF demands an increased computational complexity (since it evaluates two times of Kalman filtering).

The discrete-time EKF is stable by design, and discretization is needed only for model propagation. Since the model is stable, numerical instability is unlikely to happen, and the stability of the discrete-time model is verified. Furthermore, the importance of employing an implicit integration scheme for this case study is limited since the model (1) does not have any stiff dynamics and the simple forward Euler integration method describe the state trajectory efficiently. More detailed discussion can be found in [35]. Finally, it should be noted that if a more complicated estimation methods, that requires more time to be evaluated, an implicit integration scheme will be justified to provide the possibility of choosing a longer sampling time.

Table 2: Estimation execution time (EET) and total execution time (TET) in [ms]

Estimation methods	mean EET	mean TET	max EET	max TET
DKF	11.67	14.32	11.56	14.42
EKF	6.92	9.67	6.98	9.75

6. Conclusion

The joint state and parameter estimation problem for vibrating structures is nonlinear, even though the underlying dynamic model is linear. A globally valid LTV model describing the dynamics of a single DOF vibrating system has been prosed here, that is equivalent to the original nonlinear system.

With no input and output excitation this transformation is not well defined, while with no input excitation, but with output excitation in place, at least one of the parameters can not be estimated. These special conditions are unlikely to happen in practical applications of vibration control, while excitation may be monitored to turn off the estimation part of an adaptive-system in necessary.

The proposed LTV model was then utilized in a two stage cascaded Kalman filtering scheme known as DKF that provides a globally convergent parameter estimation in the nominal case. The performance of the DKF vibration state and parameter estimator has been then compared with the industry-standard EKF estimation method in various experimental scenarios.

The experiments presented here show, that a wrong choice of initial state and parameters; or a structural change in the underlying dynamics de-stabilizes the EKF as expected, nevertheless DKF remained convergent. Therefore, compared to EKF, we may recommend to use the cascaded DKF applications where sudden and dramatic structural changes are to be expected. The recommendation holds not only in case when state observers are used alone (e.g. structural health monitoring), but also for adaptive vibration attenuation. As our experiments demonstrate, sudden changes in structural dynamics can cause diverging EKF results, that in turn de-stabilizes control.

Since the DKF is not optimally designed for large noise amplitudes, its performance in the presence of additional measurement noise with different density functions has been studied here as well. The destructive effect of additional noise on DKF has been illustrated and compared to EKF. Even though measurement noise with a large magnitude or other than Gaussian distribution causes DKF to diverge, we observed that EKF also suffers from this issue.

Although the timing analysis analysis presented here proves the practical real-time feasibility of the proposed estimation and control on a low-cost MCU, model complexity and size is rather limited. Despite of the fact that DKF takes twice the time to execute relative to EKF, rather unsurprisingly, the absolute TETs are still quite high. Nonlinear estimation methods are computationally exceptionally demanding even for the single degree-of-freedom vibrating structure assumed here, higher frequencies and more complex models are unlikely to be real-time feasible on embedded microcontroller systems.

Acknowledgment

The authors gratefully acknowledge the contribution of the People Programme (Marie Curie Actions) of the European Union's Seventh Framework Programme (FP7/2007-2013) under REA grant agreement no. 607957 (TEMPO); the financial contribution of the STU Grant Scheme for the Support of Excellent Teams of Young Researchers, the Slovak Research and Development Agency (APVV) under the contract APVV-14-0399; the support of the Scientific Grant Agency (VEGA) of the Ministry of Education, Science, Research and Sport of the Slovak Republic under the contract 1/0144/15; the Research Council of Norway with project no. 250725, Statoil, DNV GL and Sintef through the Centers of Excellence funding scheme, project no. 223254 - Centre for Autonomous Marine Operations and Systems (NTNU-AMOS).

References

[1] B. Olofsson, J. Antonsson, H. G. Kortier, B. Bernhardsson, A. Robertsson, R. Johansson, Sensor fusion for robotic workspace state estimation, IEEE/ASME Transactions on Mechatronics 21 (5) (2016) 2236–2248.

[2] G. Takács, T. Polóni, B. Rohaľ-Ilkiv, Adaptive model predictive vibration control of a cantilever beam with real-time parameter estimation, Shock and Vibration 2014 (2014) 1–15.

[3] A. P. Ompusunggu, J. M. Papy, S. Vandenplas, Kalman-filtering-based prognostics for automatic transmission clutches, IEEE/ASME Transactions on Mechatronics 21 (1) (2016) 419–430.

[4] C. V. Rao, J. B. Rawlings, D. Q. Mayne, Constrained state estimation for nonlinear discrete-time systems: Stability and moving horizon approximations, IEEE Transactions on Automatic Control 48 (2003) 246–258.

[5] D. P. Bertsekas, Incremental least squares methods and the extended Kalman filter, SIAM Journal on Optimization 6 (3) (1996) 807–822.

[6] L. Perea, J. How, L. Breger, P. Elosegui, Nonlinearity in sensor fusion: Divergence issues in EKF, modified truncated SOF, and UKF, in: AIAA Guidance, Navigation and Control Conference and Exhibit, 2007.

[7] E. L. Haseltine, J. B. Rawlings, Critical evaluation of extended Kalman filtering and moving-horizon estimation, Industrial & engineering chemistry research 44 (8) (2005) 2451–2460.

[8] S. H. Lee, M. West, Performance comparison of the distributed extended Kalman filter and Markov chain distributed particle filter (MCDPF), IFAC Proceedings Volumes 43 (19) (2010) 151–156.

[9] M. Ficocelli, F. Janabi, Adaptive filtering for pose estimation in visual servoing, in: Intelligent Robots and Systems, 2001. Proceedings. 2001 IEEE/RSJ International Conference on, Vol. 1, 2001, pp. 19–24.

[10] M. Abdollahpouri, G. Takács, B. Rohal'-Ilkiv, Real-time moving horizon estimation for a vibrating active cantilever, Mechanical Systems and Signal Processing 86 (2017) 1–15.

[11] K. Reif, R. Unbehauen, The extended kalman filter as an exponential observer for nonlinear systems, IEEE Transactions on Signal processing 47 (8) (1999) 2324–2328.

[12] T. A. Johansen, T. I. Fossen, G. C. Goodwin, Three-stage filter for position estimation using pseudo-range measurements, IEEE Transactions on Aerospace and Electronic Systems 52 (4) (2016) 1631–1643.

[13] S. E. Azam, E. Chatzi, C. Papadimitriou, A dual kalman filter approach for state estimation via output-only acceleration measurements, Mechanical Systems and Signal Processing 60 (2015) 866–886.

[14] S. E. Azam, E. Chatzi, C. Papadimitriou, A. Smyth, Experimental validation of the kalman-type filters for online and real-time state and input estimation, Journal of Vibration and Control 23 (15) (2017) 2494–2519.

[15] T. A. Johansen, T. I. Fossen, The eXogenous Kalman filter (XKF), International Journal of Control 90 (2) (2017) 161–167.

[16] T. A. Johansen, T. I. Fossen, Nonlinear filtering with eXogenous Kalman filter and double Kalman filter, in: European Control Conference, 2016, pp. 1722–1727.

[17] M. Abdollahpouri, M. Haring, T. A. Johansen, G. Takács, B. Rohaľ-Ilkiv, Nonlinear state and parameter estimation using discrete-time double Kalman filter, in: 20th IFAC World Congress, Toulouse, 2017.

[18] E. A. Wan, R. Van Der Merwe, The unscented Kalman filter for nonlinear estimation, in: Adaptive Systems for Signal Processing, Communications, and Control Symposium, AS-SPCC, 2000, pp. 153–158.

[19] M. S. Miah, E. N. Chatzi, V. K. Dertimanis, F. Weber, Real-time experimental validation of a novel semi-active control scheme for vibration mitigation, Structural Control and Health Monitoring 24 (3).

[20] M. S. Miah, E. N. Chatzi, F. Weber, Semi-active control for vibration mitigation of structural systems incorporating uncertainties, Smart Materials and Structures 24 (5) (2015) 055016.

[21] F. Piovanelli, P. Paoletti, G. Innocenti, Enhanced nonlinear model and control design for a flexible wing, in: European Control Conference (ECC), 2016, pp. –.

[22] N. P. Jones, T. Shi, J. H. Ellis, R. H. Scanlan, System-identification procedure for system and input parameters in ambient vibration surveys, Journal of Wind Engineering and Industrial Aerodynamics 54 (1995) 91–99.

[23] V. Namdeo, C. Manohar, Nonlinear structural dynamical system identification using adaptive particle filters, Journal of Sound and Vibration 306 (3) (2007) 524–563.

[24] K. J. Åström, T. Bohlin, Numerical identification of linear dynamic systems from normal operating records, in: Theory of Self-Adaptive Control Systems, Plenum Press, 1966, pp. 96–111.

[25] A. H. Jazwinski, Stochastic processes and filtering theory, Courier Corporation, 2007.

[26] G. Folland, Remainder estimates in Taylor's theorem, The American Mathematical Monthly 97 (3) (1990) 233–235.

[27] J. A. Mynderse, G. T.-C. Chiu, Two-degree-of-freedom hysteresis compensation for a dynamic mirror actuator, IEEE/ASME Transactions on Mechatronics 21 (1) (2016) 29–37.

[28] H. Li, C. Du, Y. Wang, Optimal reset control for a dual-stage actuator system in HDDs, IEEE/ASME Transactions on Mechatronics 16 (3) (2011) 480–488.

[29] J. B. Rawlings, K. R. Muske, The stability of constrained receding horizon control, IEEE transactions on Automatic Control 38 (10) (1993) 1512–1516.

[30] P. Dorato, A. Levis, Optimal linear regulators: The discrete-time case, IEEE Transactions on Automatic Control 16 (6) (1971) 613–620.

[31] D. S. Naidu, Optimal control systems, CRC press, Boca Raton, FL, 2002.

[32] J. Richelot, J. Bordeneuve-Guibe, V. Pommier-Budinger, Active control of a clamped beam equipped with piezoelectric actuator and sensor using generalized predictive control, in: 2004 IEEE International Symposium on Industrial Electronics, Vol. 1, 2004, pp. 583–588 vol. 1.

[33] C. Vasques, J. D. Rodrigues, Active vibration control of smart piezoelectric beams: comparison of classical and optimal feedback control strategies, Computers & structures 84 (22) (2006) 1402–1414.

[34] A. Grewal, V. Modi, Robust attitude and vibration control of the space station, Acta Astronautica 38 (3) (1996) 139 – 160.

[35] G. Takács, T. Polóni, B. Rohaľ-Ilkiv, Pseudo real-time state and parameter estimation of a vibrating active cantilever using the moving horizon observer, in: Proceedings of the 21th International Congress on Sound and Vibration (ICSV 14), Beijing, China, 2014, pp. 820/1–820/8.

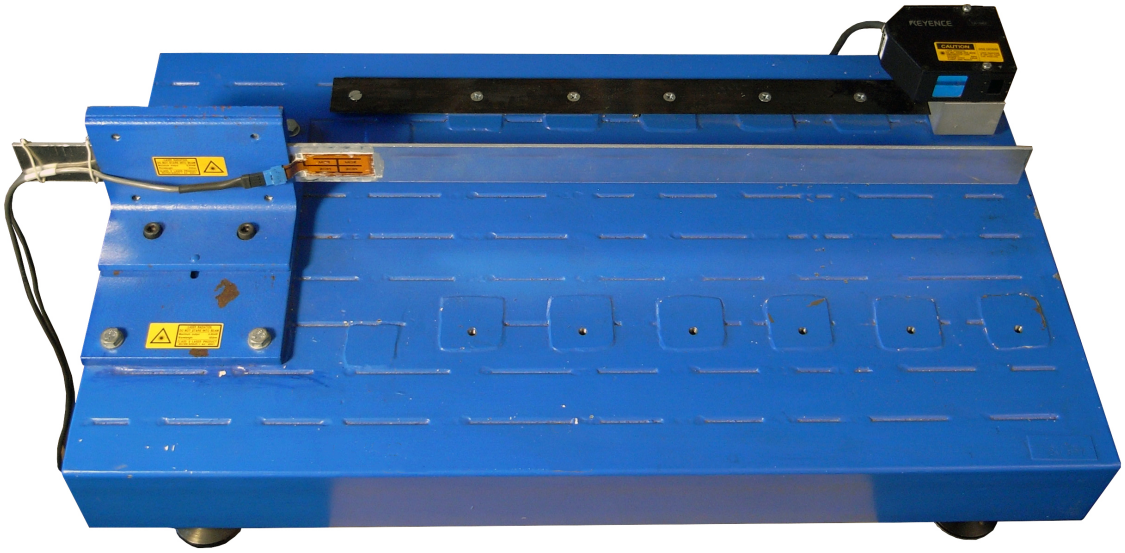

(a) Cantilever beam assembly

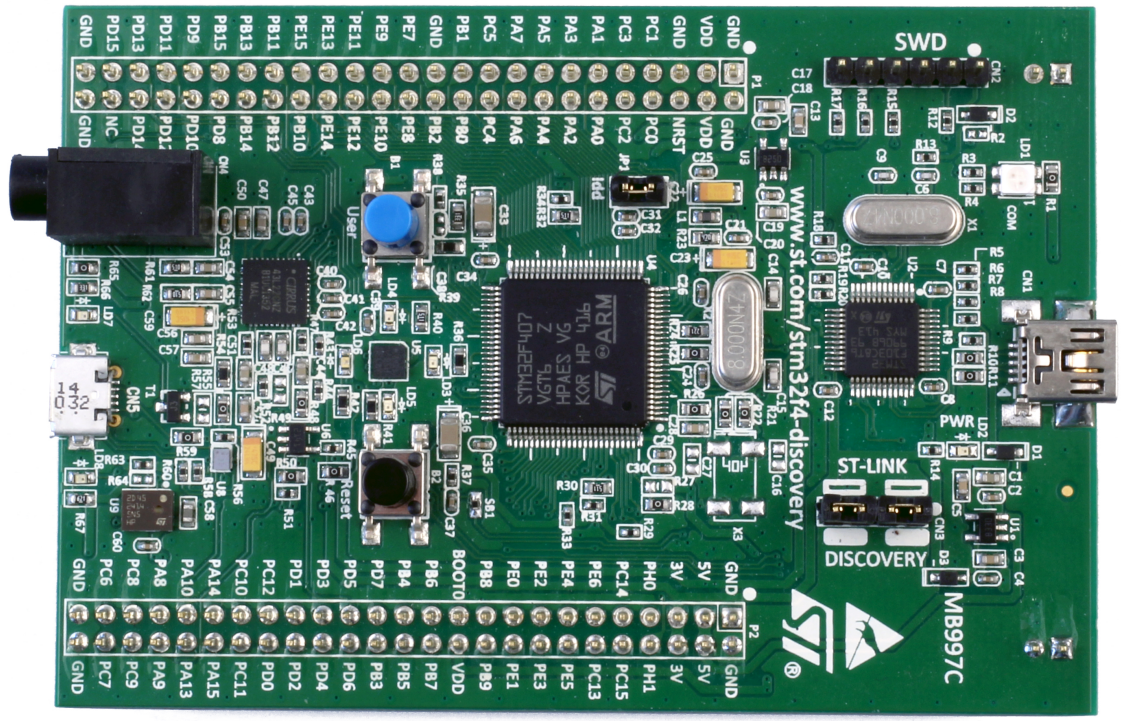

(b) STM32F407 Discovery Evaluation Board

Figure 2: Equipment used in the experiment

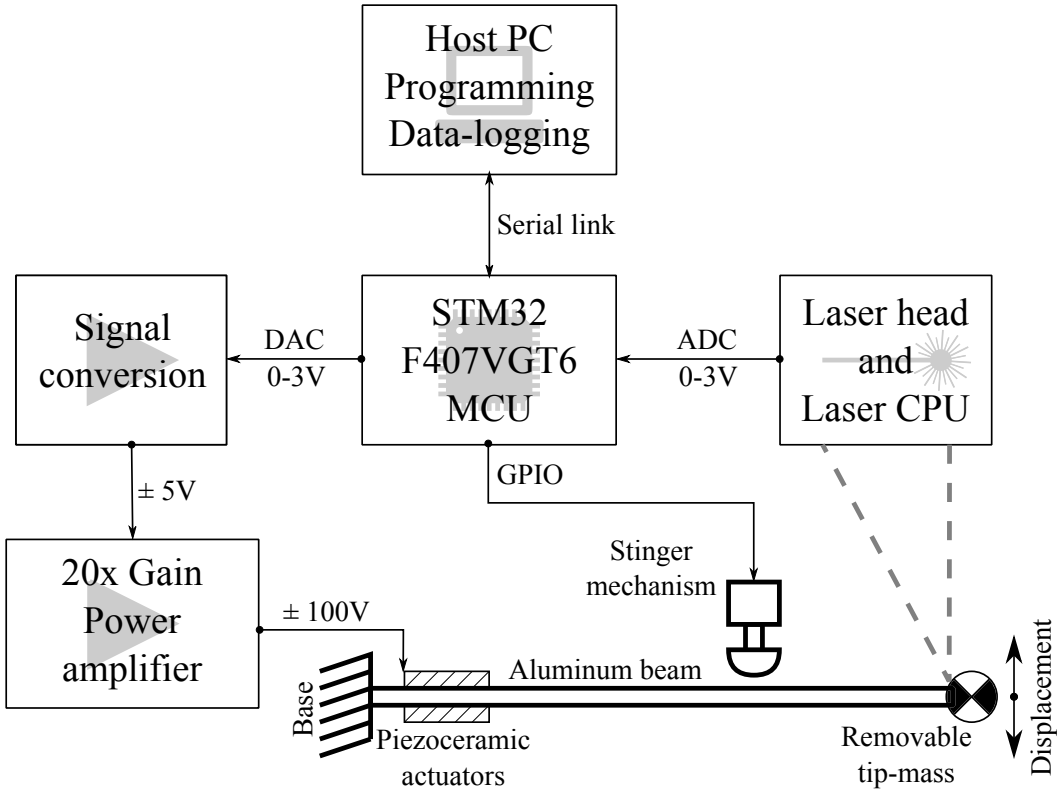

(a) Scheme of the experimental hardware setup

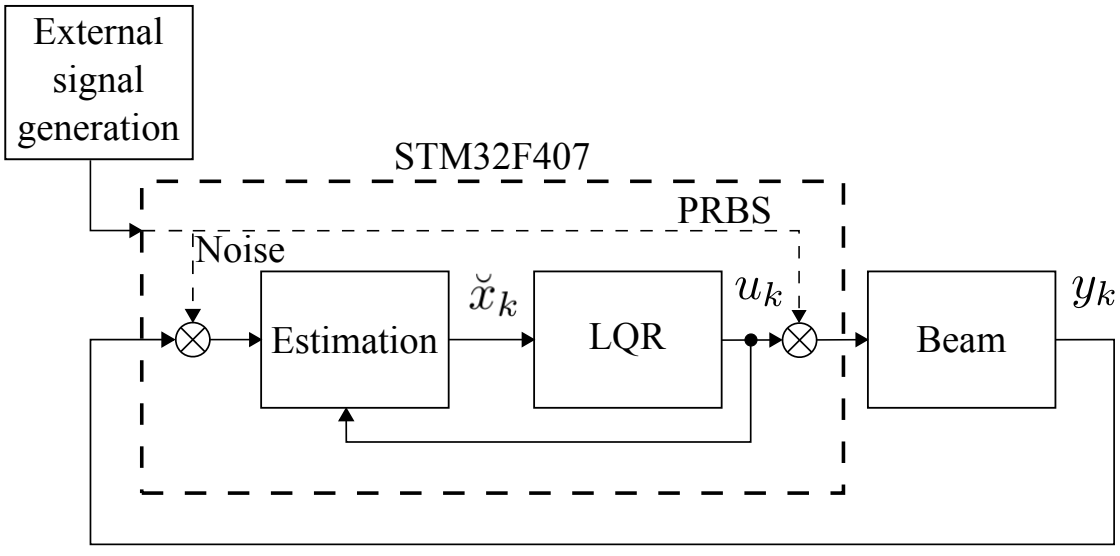

(b) Closed-loop implementation scheme

Figure 3: Implementation schemes

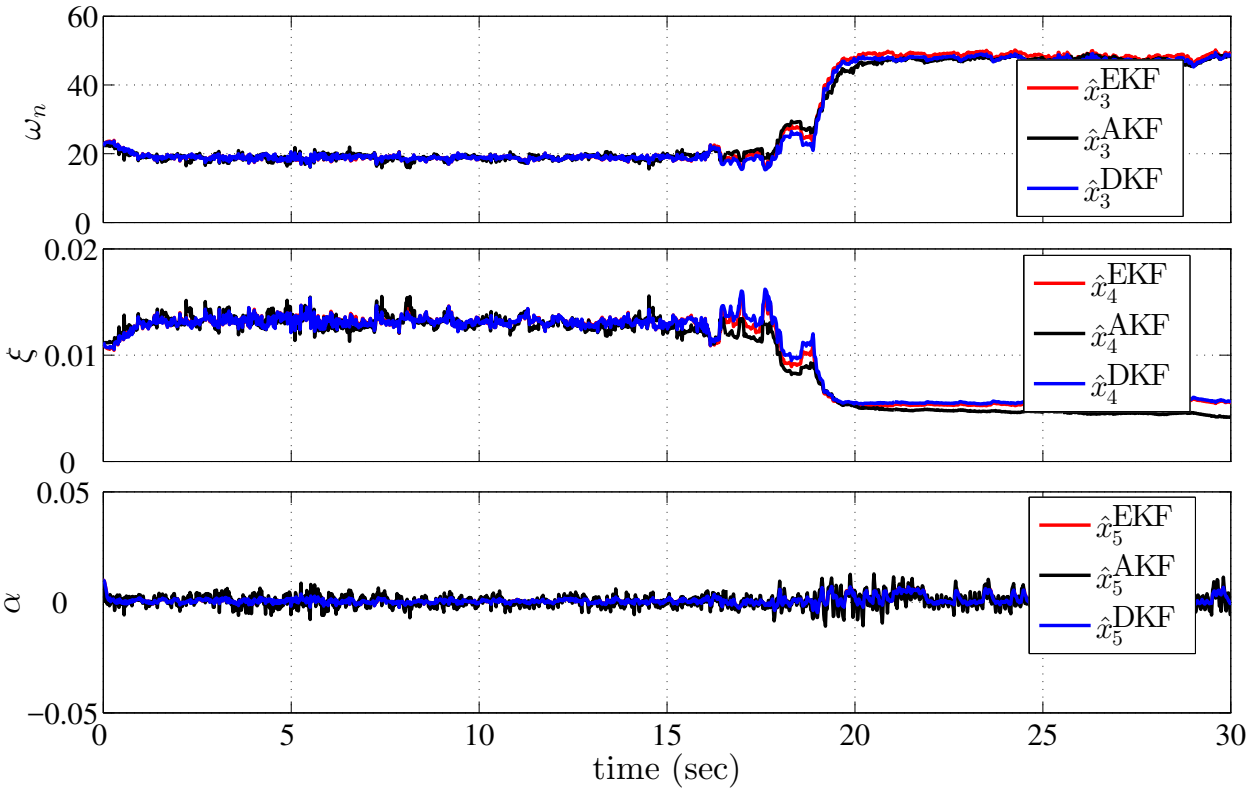

(a) proper initial guess is provided

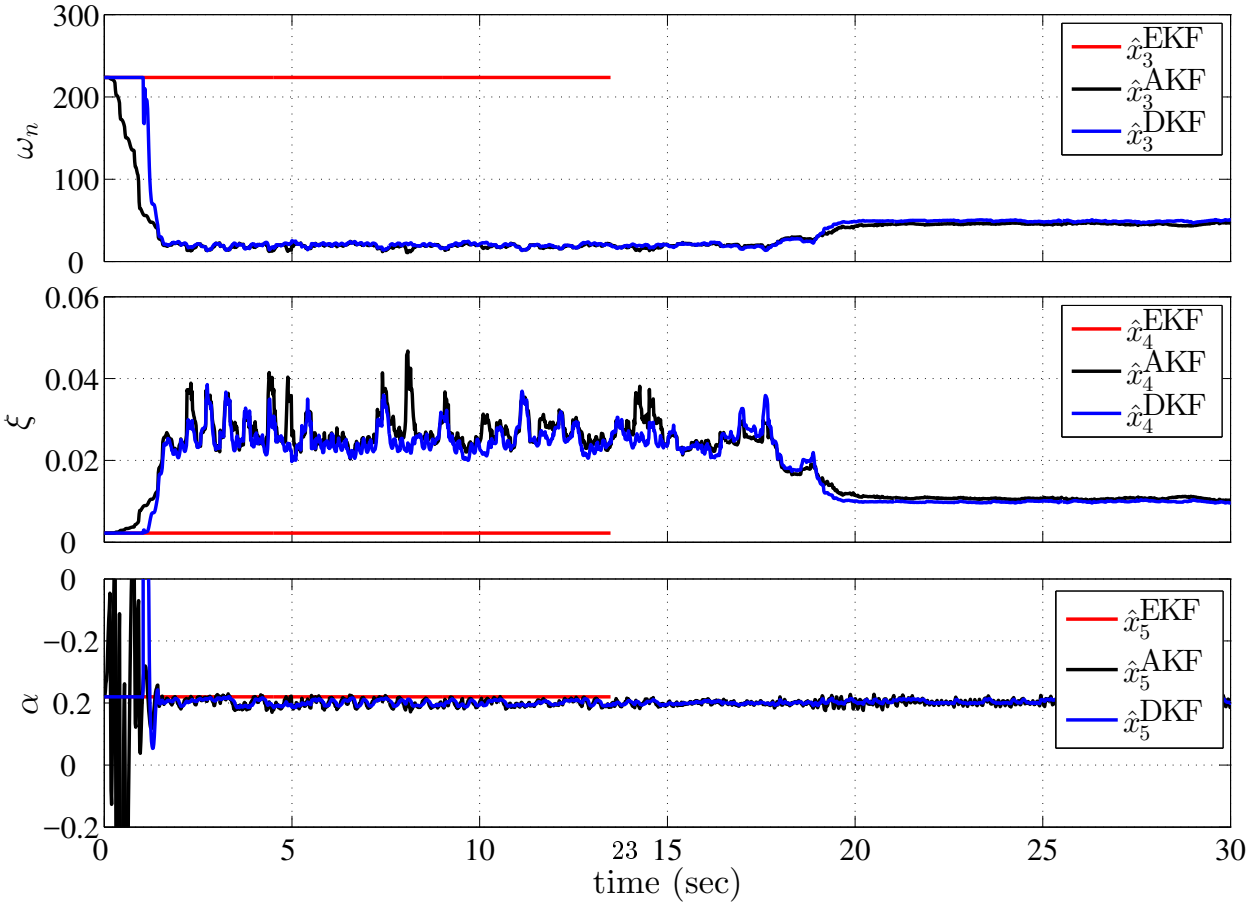

(b) wrong initial guess is provided

Figure 4: Parameters estimation result with large tip mass change

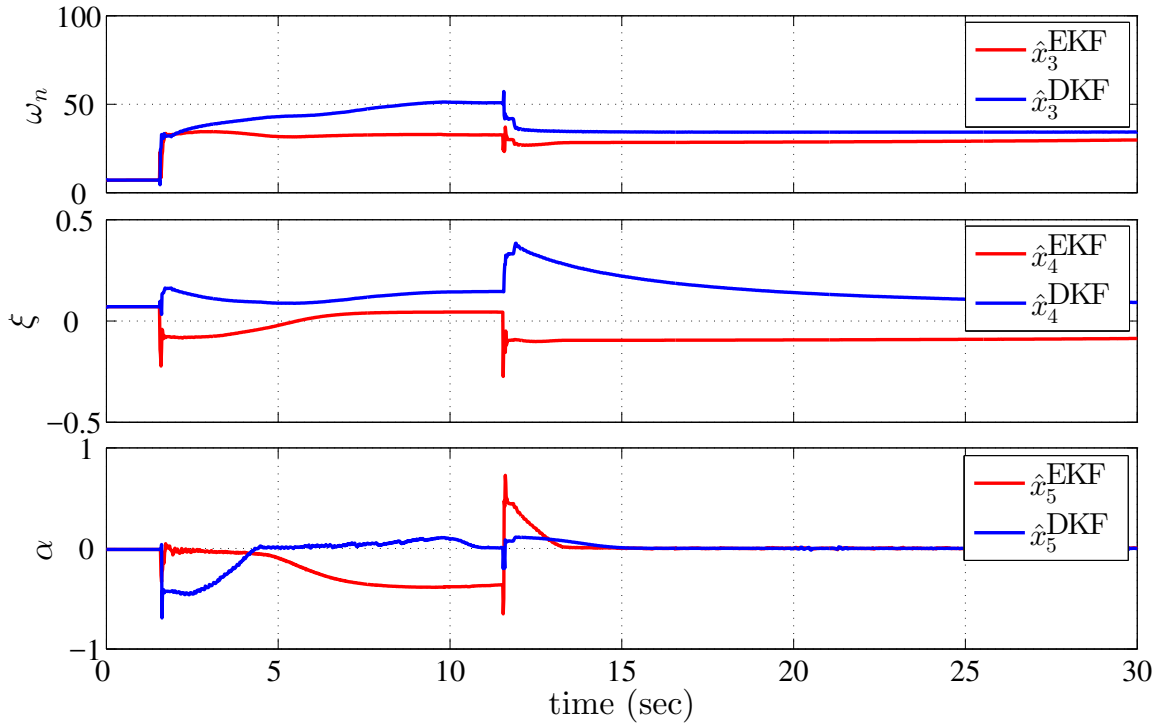

(a) Parameter estimation for LQR

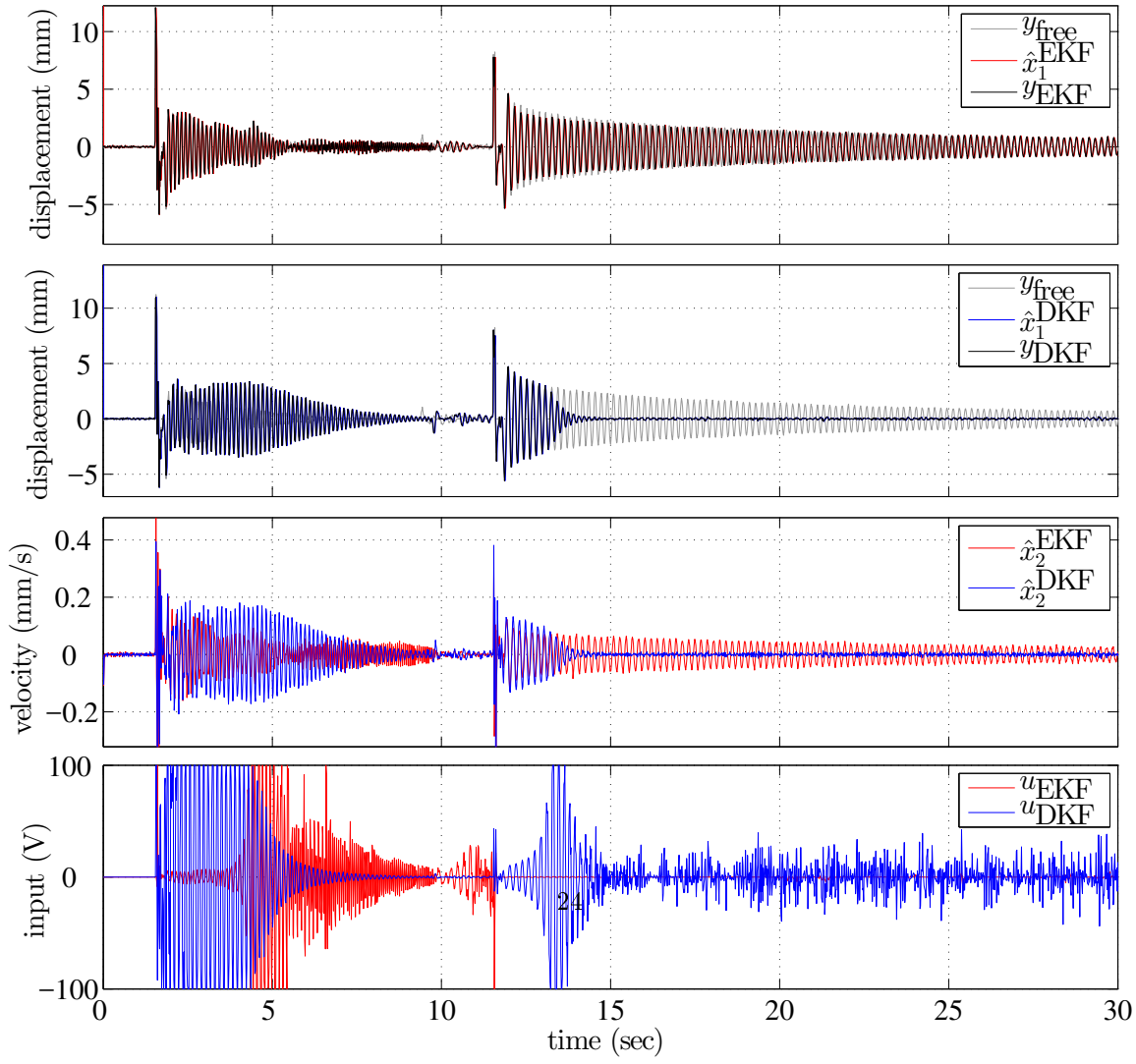

(b) State estimations and attenuation results with LQR

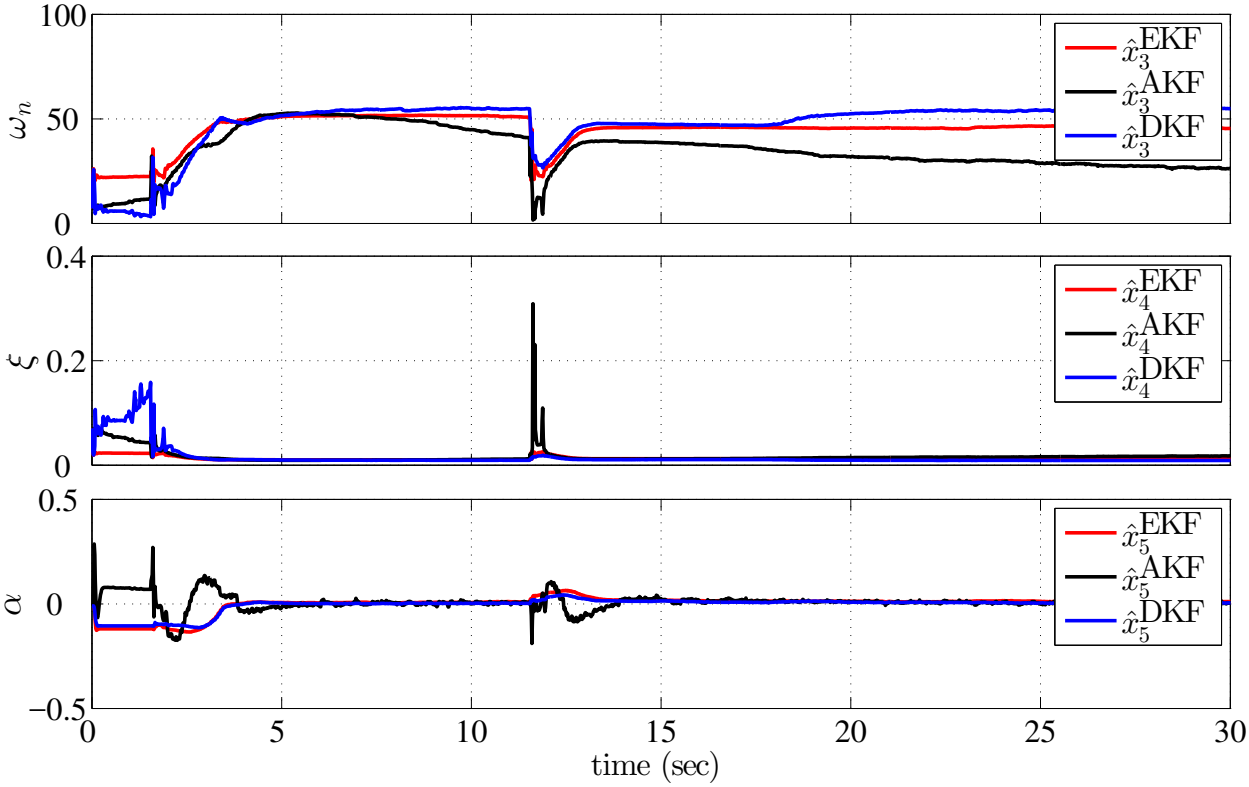

Figure 6: Estimated parameters with additive Gaussian measurement noise

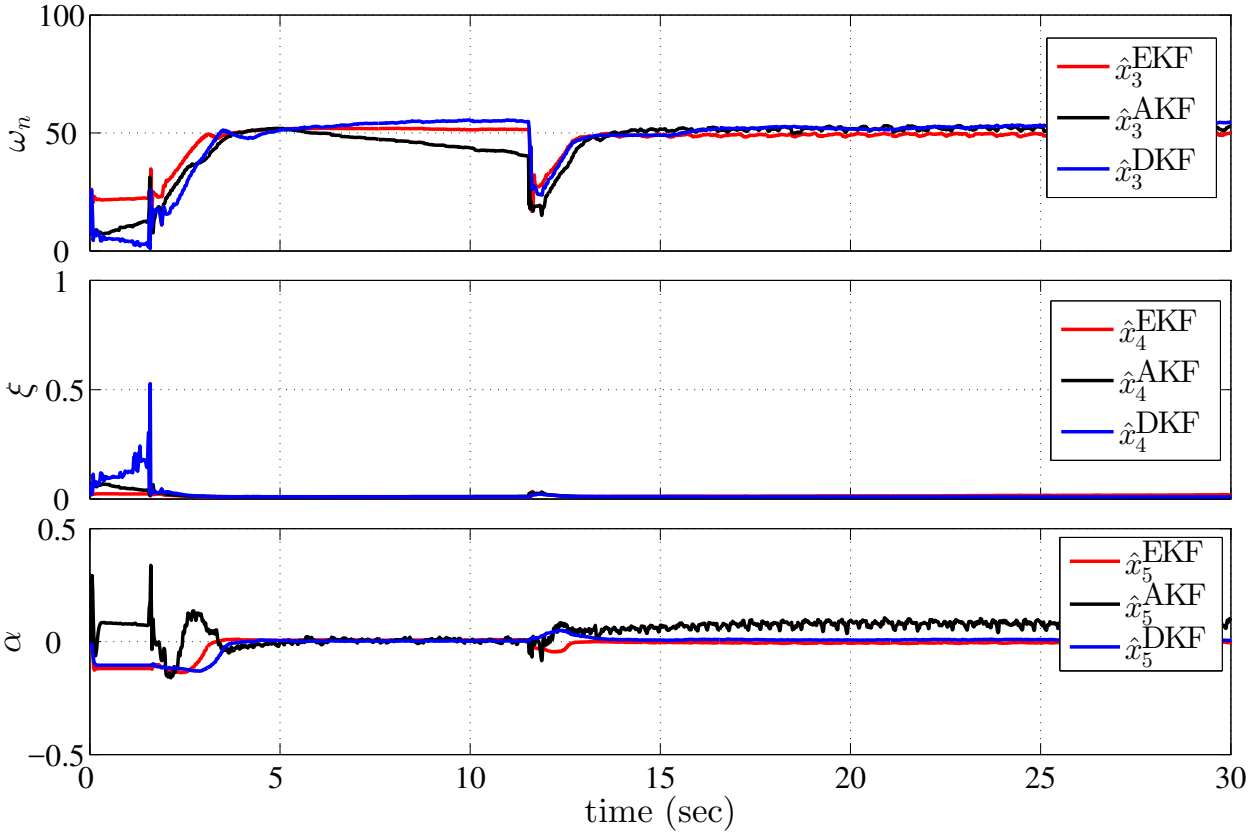

Figure 7: Estimated parameters with additive uniform measurement noise